J. Fluid Mech. (2023), *vol*. 958, A34, doi:10.1017/jfm.2023.118

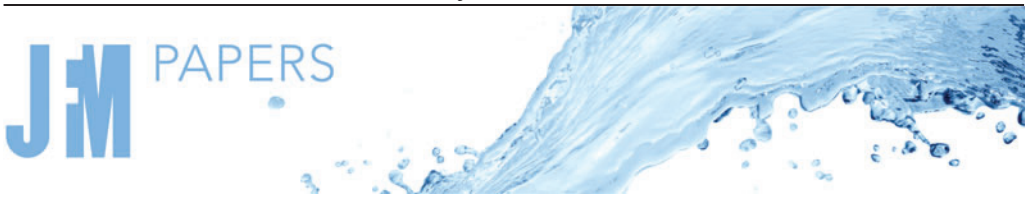

Viscoplastic lines: printing a single filament of yield stress material on a surface

Jesse van der Kolk[1], **Daniël Tieman**[1] **and Maziyar Jalaal**[1,†]

[1]Van der Waals–Zeeman Institute, University of Amsterdam, Science Park 904, 1098 XH Amsterdam, The Netherlands

(Received 23 January 2022; revised 26 December 2022; accepted 29 January 2023)

This study presents the spreading of a single filament of a yield stress (viscoplastic) fluid extruded onto a pre-wetted solid surface. The filaments spread laterally under surface tension forces until they reach a final equilibrium shape when the yield stress dominates. We use a simple experimental set-up to print the filaments on a moving surface and measure their final width using optical coherence tomography. Additionally, we present a scaling law for the final width and determine the corresponding prefactor using asymptotic analysis. We then analyse the level of agreement between the theory and experiments, and discuss the possible origins of discrepancies. The process studied here has applications in extrusion-based thermoplastic and bio-three-dimensional printing.

Key words: drops

1. Introduction

Spreading of non-Newtonian liquids on surfaces is of widespread interest in many fabrication, coating and printing applications (Derby 2010; Mackay 2018; Lohse 2022). Among them are the extrusion-based three-dimensional (3-D) printing techniques, where digitally designed objects are built via line-by-line and then layer-by-layer deposition of ink through a nozzle. A diverse range of materials can be used in 3-D printing for various manufacturing purposes, from soft tissues and synthetic bones in biomedical applications (Placone & Engler 2018) to food pastes (Zhu *et al.* 2019), energy materials (Tagliaferri, Panagiotopoulos & Mattevi 2021) and ceramics (Faes *et al.* 2015). These materials, depending on the application, are printed as single filament or monolayer (e.g. for conductive circuit printing; Postiglione *et al.* 2015; Zhang *et al.* 2016; Gnanasekaran

† Email address for correspondence: m.jalaal@uva.nl

et al. 2017; Valino *et al.* 2019) or, more commonly, with multilayer printing (Lewis 2006; Ngo *et al.* 2018). The characteristics of the single-line depositions can influence directly the product quality for single-filament printing, and can also affect the overall quality of multilayer printing via setting up the first-layer deposition. Hence understanding the underlying physics of deposition of a single line of inks and the effects of rheological properties is essential to improve the design of extrusion-based 3-D printers or to design new inks based on the rheology of complex fluids (Ewoldt & Saengow 2021). We will address the deposition of a single filament of viscoplastic (or yield stress) fluids. Such materials are neither solids nor liquids. When the external stress is below the yield stress, the material behaves effectively like an elastic solid, but when the stress exceeds the yield stress, the material deforms plastically and flows like a viscous liquid (Barnes 1999; Coussot 2014; Balmforth, Frigaard & Ovarlez 2014; Bonn *et al.* 2017). Viscoplasticity is a common feature of many industrial fluids, such as waxy oil and cosmetic and dairy products. Furthermore, viscoplastic fluids represent a large group of polymeric inks used in 3-D printing (Lewis 2006; O'Bryan *et al.* 2017), where, depending on the application, the values of the ink's yield stress varies (M'barki, Bocquet & Stevenson 2017; Paxton *et al.* 2017; Siqueira *et al.* 2017; Eom *et al.* 2019; Kiyotake *et al.* 2019; del Mazo-Barbara & Ginebra 2021; Siacor *et al.* 2021). While many inks feature a relatively large yield stress of hundreds of pascals, many others are much softer, with yield stress in tens of pascals. Examples of the latter category can be found in conductive inks and energy materials used in direct writing (Zhang *et al.* 2016; Tagliaferri *et al.* 2021), bioprinting hydrogels (Rodell, Kaminski & Burdick 2013; Mouser *et al.* 2016; Wilson *et al.* 2017), kaolin-based materials (Sun *et al.* 2018), colloidal inks (Eom *et al.* 2019) and cellulose suspension (Jiang *et al.* 2020). The main focus of the present work is to study the spreading of such soft viscoplastic inks, where the values of yield stress are comparable with the driving spreading stresses.

Spreading and deposition of viscoplastic fluids share similarities and also present different characteristics in comparison to Newtonian fluids (Bonn *et al.* 2009). Like Newtonian (and viscoelastic) fluids, viscoplastic fluids (if soft enough) spread due to surface tension and gravity, on time scales associated with the apparent viscosity. The most distinctive trait of viscoplastic spreading, however, might manifest in the final shape. Theoretically, a Newtonian free-surface flow on a fully wetting surface spreads (due to gravity or surface tension) until it is finally completely flat (Tanner 1979; Tuck & Schwartz 1990; Backholm *et al.* 2014; Bergemann, Juel & Heil 2018; Jalaal, Seyfert & Snoeijer 2019*c*). In contrast, in the same situation, a viscoplastic fluid eventually stops at a finite time, when the stress everywhere inside the material falls below the yield stress. Hence, contrary to a Newtonian liquid, a viscoplastic liquid reaches a characteristic final shape (Dubash *et al.* 2009; Liu *et al.* 2016; Jalaal, Stoeber & Balmforth 2021) on a fully wetting surface. Finding the final shape for spreading viscoplastic filaments is indeed the main objective of this study. Note that in practice, it might be difficult to distinguish the deposition behaviour of a viscoplastic fluid from a highly viscous Newtonian fluid or a viscoelastic liquid with long characteristic elastic time scales. Moreover, the final shape of the complex fluid could be affected by other factors such as time-dependent material properties like thixotropy (Uppal, Craster & Matar 2017; Oishi, Thompson & Martins 2019*b*; Sen, Morales & Ewoldt 2021) and solidification (Tavakoli, Davis & Kavehpour 2014; Jalaal *et al.* 2018; Koldeweij *et al.* 2021).

The present study relates to a number of previous research lines in the literature. One is the gravity-driven spreading and large-scale 3-D printing of yield stress materials, in particular concrete (Roussel & Coussot 2005; Flatt, Larosa & Roussel 2006; Ancey

2007; Liu *et al.* 2016; Gosselin *et al.* 2016; Buswell *et al.* 2018; Garg *et al.* 2021; Valette *et al.* 2021). The major differences between the present study and these works are the characteristic length scales and the driving mechanisms. While gravity is the main force of spreading in large-scale 3-D printers, surface tension is the dominant factor at a small scale or when gravity is absent (Brutin *et al.* 2009; Diana *et al.* 2012; D'Angelo *et al.* 2022). This changes the underlying physics, where the competition of yield stress and capillary forces determines the final shape of the liquid. We refer to the phenomenon of capillary-driven yield stress fluids as plastocapillarity. Also related to the present study are the previous investigations on the impact and spreading of viscoplastic droplets on dry and wet surfaces (Luu & Forterre 2009; German & Bertola 2010; Saïdi, Martin & Magnin 2010; Blackwell *et al.* 2015; Jalaal, Balmforth & Stoeber 2015; Oishi, Thompson & Martins 2019*a*; Oishi *et al.* 2019*b*; Martouzet *et al.* 2021; Sen *et al.* 2021), where, depending on the regime parameters, different factors such as inertia, elasticity, gravity, thixotropy and surface tension can determine the dynamics of the droplets. In the present work, we will focus on a different geometry (filaments) on a small scale, and a regime and type of material where surface tension and yield stress effects dominate.

To address the problem, we will use experimental and theoretical tools. The paper is organized as follows. Section 2 presents the experimental details, including the set-up and the used fluids. Section 3 provides the results, a simple scaling law, and a more detailed description of the empirical observations based on viscoplastic lubrication theory. Section 4 concludes the results and presents future perspectives.

2. Experiments

2.1. *Set-up*

The experimental set-up is a 'simplified 3-D printer' (see figure 1). The fluid was injected, using a syringe pump, at a constant rate Q through a hydrophobic nozzle with inner diameter 0.912 mm. The substrate was a glass plate, pre-wetted with a thin layer of the same fluid at constant height $h_\infty \approx 40$ μm. The pre-wetting layer not only simulates the condition of a fully wetted surface but also allows us to avoid any complexity due to the (triple) contact line (Oron, Davis & Bankoff 1997; Craster & Matar 2009; Jalaal *et al.* 2021; Martouzet *et al.* 2021). Pre-wetting was done just before the experiments to minimize evaporation effects. The distance between the nozzle and the surface of the pre-wetted film was fixed at 350 ± 10 μm. Changing this distance by 75–400 μm did not change the results. The substrate was placed on a linear motor (Thorlabs LTS300/M). When the flow is established through the nozzle, the linear motor moves (constant velocity $U = 10$ mm s^{-1} and initial acceleration 50 mm s^{-2}) and a viscoplastic line begins to form on the surface. The substrate motion continued until a line of length 80 ± 2 mm was obtained. Note that the short delays between the pump's function and the substrate's motion disturb the filament's shape at the beginning and end (∼5 mm on each side). We perform the measurements far from these areas. Also, measurements were performed 20 s after the deposition to ensure that the final equilibrium shape was obtained. As the line is printed, it travels under a lens of an optical coherence tomography (OCT) scanner to obtain the shape of the interface. OCT is a non-invasive optical technique that uses low-coherence interferometry to obtain depth scans (Fercher *et al.* 2003). A series of these depth scans is then used to form a cross-sectional image. The technique has been used to study evaporating droplets (Edwards *et al.* 2018), flow inside channels (Daneshi *et al.* 2019), and spreading and solidification of droplets of complex fluids (Jalaal *et al.* 2018). The current

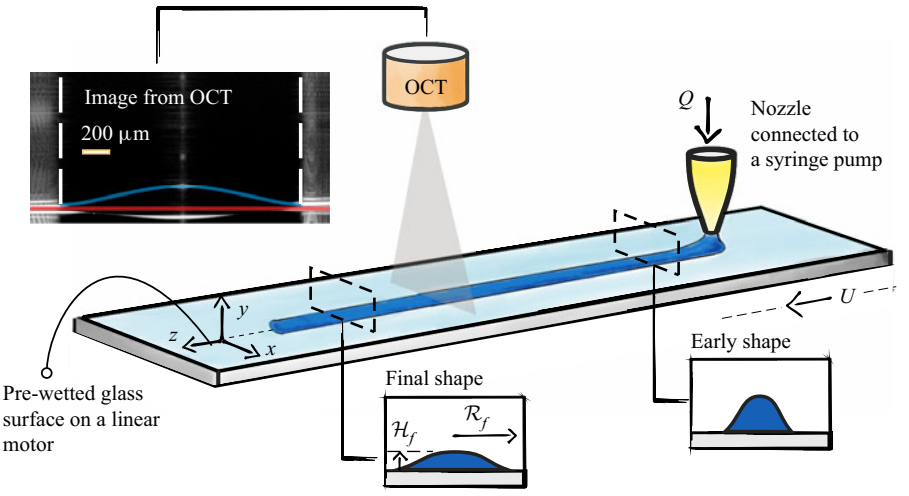

Figure 1. Experimental set-up for the investigation of printing a single line of viscoplastic fluids. The shown dimensions in the schematic are not to scale. A filament of a yield stress (viscoplastic) fluid is printed on a moving pre-wetted substrate. After extrusion from the nozzle, the filament spreads on the surface until it reaches a final width. We denote the final half-width of the filament as $\mathcal{R}_f$. An optical coherence tomography (OCT) scanner is used to measure the final width of the filaments. An example of the OCT image is shown in the top-left of this figure, where blue and red lines highlight the interface of the filament and the substrate. The dashed vertical lines show the edge of the filament, where the surface becomes flat.

experimental set-up did not allow for an accurate measurement of dynamic of spreading. Nonetheless, using OCT provides many advantages for our system. In the set-up, the flat pre-wetted film, unlike the curved surface of the printed line, forms high-intensity patterns of vertical lines. This is due to the over-saturation of the reflected light on a flat surface. Hence, by detecting the edge of these patterns (vertical dashed white lines in figure 1), we were able to obtain easily the width of the filament with accuracy $O(10\ \mu\text{m})$. Furthermore, by adding microparticles (3 μm polystyrene from microparticles GmbH) to the fluid, we were able to roughly inspect the flow inside the printed lines and ensure that the flow along the length of the filament (z-direction in figure 1) was negligible, and therefore the spreading was mainly across the width (x–y plane in figure 1). Experiments were repeated at least 10 times for each data point (total of ∼300 experiments). All measurements were performed at steady state when the filaments had reached their final shape. For each experiment, the OCT scans were performed for four cross-sections of the line, and the values were averaged.

2.2. *Fluids*

We used a mixture of Milli-Q water and a commercial hair gel at five different concentrations. The final materials are basically aqueous mixtures of Carbopol that are pH-neutralized with triethanolamine (Dinkgreve *et al.* 2016). The samples were centrifuged before the experiments to remove bubbles. An Anton Paar MCR 302 rheometer with a rough cone-and-plate configuration (2° angle) was used to characterize the rheological properties of the liquids. For each sample, we obtained the steady-state flow curves as well as viscoelastic response in an oscillatory shear test. Figure 2 shows an example of measurements for one of the samples. Similar to what has been reported previously (Kim *et al.* 2003; Dinkgreve *et al.* 2016; Jalaal *et al.* 2019*b*), the fluids show

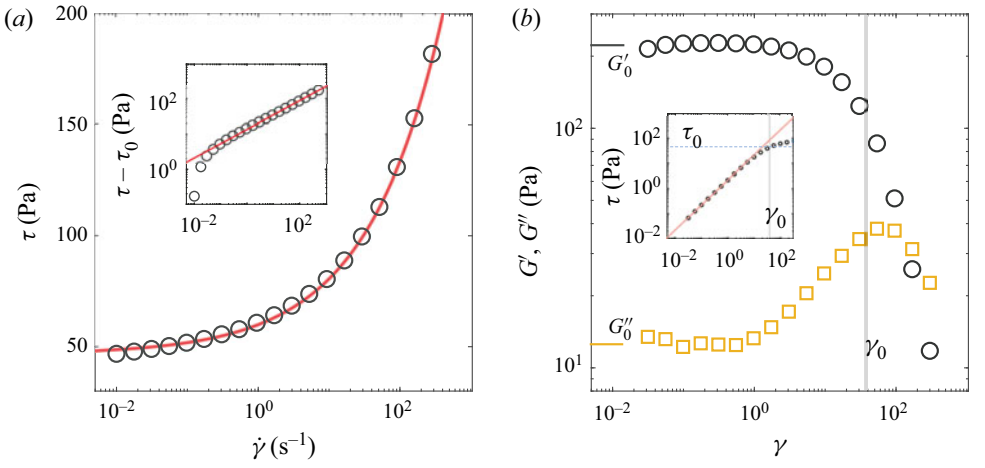

Figure 2. (*a*) Flow curve (shear stress versus shear rate) for sample 4 (see table 1). The inset shows the viscous stress ($\tau - \tau_0$) versus the shear rate. The symbols are the measurements, and the red lines are the corresponding Herschel–Bulkley fits. (*b*) Storage modulus (G', circles) and loss modulus (G'', squares) for sample 3 as a function of strain. The vertical grey line shows the critical strain at which stress is equal to the yield stress (from the Herschel–Bulkley fit). The inset shows the variation of shear stress versus the strain. The red line is a linear fit with the slope $G'_0 \approx 223$. The normal lines highlight the critical strain and the yield stress.

Sample	τ_0 (Pa)	K (Pa s^n)	n	G'_0 (Pa)	G''_0 (Pa)
1	102.0	34.3	0.39	365	22.9
2	84.2	27.9	0.40	327	20.4
3	66.2	21.1	0.40	282	19.6
4	46.6	13.33	0.41	223	13.2
5	29.8	8.57	0.42	149	8.8
6	4.0	1.46	0.51	25.1	1.7

Table 1. Values of yield stress τ_0, consistency index K, shear index n, small strain elastic modulus G'_0 and loss modulus G''_0.

a Herschel–Bulkley-type behaviour where the viscosities drop with the shear rate, and at low shear rates, the stress values converge to the yield stress. We therefore characterize the material properties by fitting the following equations to the flow curves (see figure 2*a*):

$$\tau - \tau_0 = K\dot{\gamma}^n, \tag{2.1}$$

where τ_0 is the yield stress, K is the consistency index, and n is the shear index. The fitting values for six samples are listed in table 1. Oscillatory tests reveal the elastic-dominated behaviour at low strains/stresses with almost constant elastic and loss moduli. We quantified these values by averaging the values of G' and G'' at a small strain region, when $\gamma < 1$ (see table 1). At large deformations, when stress exceeds the yield stress, the values of G' and G'' drop significantly, and the material behaves mostly like a viscous fluid with weak elasticity (see also Donley *et al.* 2020).

The densities of the fluids (ρ) are almost the same as for water (Jalaal *et al.* 2019*b*). Like other yield stress fluids, the surface tension of the materials (σ) is hard to measure. Previous attempts in the literature (Jørgensen *et al.* 2015) mostly report slightly smaller

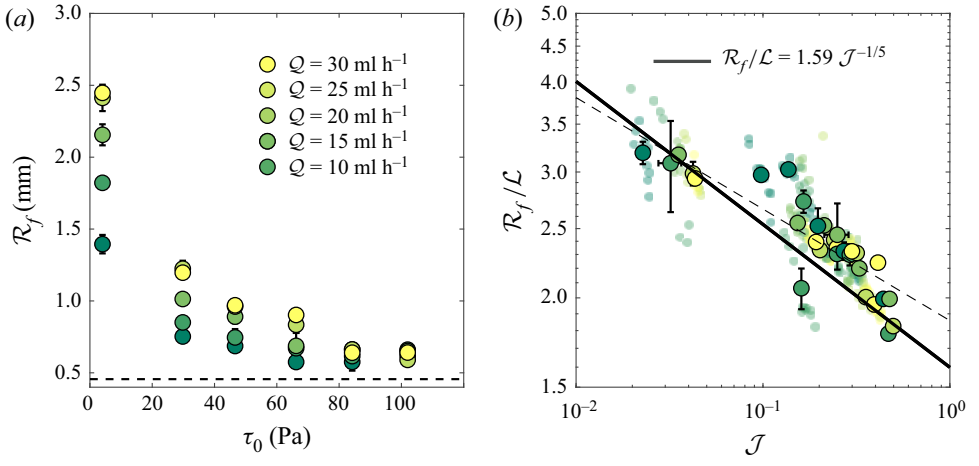

Figure 3. (*a*) Dimensional final half-width of the printed line for different flow rates and yield stress values. The dashed line shows the radius of the nozzle (≈0.46 mm). (*b*) Dimensionless half-width of the lines as a function of the plastocapillary number $\mathcal{J}$. The experimental repetitions data are plotted as small transparent points, and the large circles are the average values with standard deviations as the error bars. Equation (3.3) is plotted as the solid line. The dashed line is a power-law fit through the experiments, $\mathcal{R}_f/\mathcal{L} = 1.859\mathcal{J}^{-0.156}$.

values than the surface tension of water. We therefore use $\sigma = 0.072$ N m^{-1} in our calculations, but one should take this value likely as an upper bound.

3. Analysis

The experimental results for the final half-width of the filament $\mathcal{R}_f$, for different flow rates $\mathcal{Q}$ and yield stresses τ_0, are shown in figure 3(*a*). As the yield stress increases, the filaments spread less, hence the values of $\mathcal{R}_f$ reduce. Meanwhile, for a given yield stress value, a larger flow rate results in a larger deposited volume of the filament and therefore larger $\mathcal{R}_f$. The latter is more pronounced when the yield stress is small. When the value of yield stress is large, the filament is less affected by the surface tension, after the extrusion from the nozzle. Therefore, the final half-width of the filament approaches the radius of the nozzle (shown by the horizontal dashed line).

The experimental conditions were selected such that the filaments' cross-sectional features are small compared to the capillary length scale $l_c = (\sigma/\rho g)^{1/2}$. We define the characteristic length scale of the filament as $\mathcal{L} = \sqrt{A}$, where $A(Q, U)$ is the cross-sectional area of the filament obtained by processed OCT images. Depending on the fluid and Q, the values of $\mathcal{L}$ vary between 0.2 mm and 0.9 mm. The filaments were deposited at relatively low flow rates, $Q = 10$–30 ml h^{-1}. Given the high apparent viscosity of the liquids and small characteristic length scales of the filaments, the inertial effects are negligible. To this end, one could define a Reynolds number for a Herschel–Bulkley fluid (Jalaal, Kemper & Lohse 2019*a*) as $Re = \rho U^2/(K(U/\mathcal{L})^n + \tau_0)$, which compares the inertial and (apparent) viscous forces, and also a Weber number $We = \rho U^2 \mathcal{L}/\sigma$, which compares inertial and capillary forces. For the experimental parameters here, $Re \sim We \sim O(10^{-4})$, showing the negligible inertial effects. Additionally, the small size of the filaments suggests that the gravitational effects are also relatively small in comparison with the surface tension effects. The latter could be seen in small values of the Bond number ($Bo = \rho g \mathcal{L}^2/\sigma$, with,

$0.01 < Bo < 0.13$), which compares the pressure due to the gravitational acceleration (g) to capillary pressures. The importance of elastic effects is less obvious, given the large nonlinear variation of viscoelastic properties of the liquid under different strains (see figure 2*b*). An estimation for the elastic time scale can be made as $\lambda \approx (K/G')^{1/n}$ (Bird, Armstrong & Hassager 1987; Luu & Forterre 2009). For G' at the critical strain γ_0, when stress is close to the yield stress, we measure $\lambda \approx 0.1$–1 s. In our experimental set-up, it takes 7–12 s for filaments to spread fully on the surface. Hence the elastic time scales are smaller than the experimental time scales, suggesting that the elastic effects might be small. Note that such a rough comparison of time scales does not necessarily show that elasticity has no effect on the dynamics and final shape of the filament. We will discuss this further in § 4. However, a rough comparison of relaxation time scales and the experimental time scales suggests that, at least to a first approximation, the elastic effects are small for the range of experimental conditions here. Hence the final width of the filament is a function of the yield stress τ_0, surface tension coefficient σ, and the flow rate Q. The latter, in our set-up, determines mainly the volume of the line ($\sim A$). Therefore, the final width can be found to be a function of a single dimensionless group, namely the plastocapillary number

$$\mathcal{J} = \frac{\tau_0 \mathcal{L}}{\sigma}. \tag{3.1}$$

This number determines the yield stress ratio to the characteristic capillarity pressure. As the plastocapillary number increases, the plasticity effects become more pronounced compared to the capillary pressure, hence one can expect a line with a smaller width. In the context of 3-D printers, for a millimetric filament with surface tension close to that of water, the capillary pressure is $O(10\ \text{Pa})$, meaning that inks with yield stress $O(10\ \text{Pa})$ or smaller are soft enough to spread easily on the surface. If $\mathcal{J} \gg 1$, then one could expect a very stiff filament that sustains its shape after extruding from the nozzle. This means that $\mathcal{R}_f/\mathcal{L} \to 1/\sqrt{\pi}$ when $\mathcal{J} \to \infty$.

Figure 3(*b*) shows the normalized value of the final half-width of filaments ($\mathcal{R}_f/\mathcal{L}$) versus the plastocapillary number for all collected experimental data. The normalized data suggest a power-law relationship between $\mathcal{R}_f/\mathcal{L}$ and $\mathcal{J}$. We attempt to find this relationship in the following.

3.1. *Scaling law*

Consider a viscoplastic filament that is spreading under capillary actions and comes to a halt due to the yield stress. The final shape of such a filament could be approximated by balancing the forces acting on the filament (Jalaal *et al.* 2021). In this case, the driving force (F_σ) is due to the capillary action, and the resisting force is due to the yield stress (F_{τ_0}), acting mainly on the base of the filament. These forces can be estimated as

$$F_\sigma = \sigma \kappa \mathcal{H}_f b \quad \text{and} \quad F_{\tau_0} = \tau_0 \mathcal{R}_f b, \tag{3.2a,b}$$

where $\mathcal{H}_f$ is the final height of the filament, $\kappa \approx \mathcal{H}_f/\mathcal{R}_f^2$ is a characteristic curvature, and b is the length of the filament. The cross-sectional area of the filament could be estimated as $A = \mathcal{L}^2 \sim \mathcal{H}_f \mathcal{R}_f$. Using this, and balancing the forces in (3.2*a*,*b*), we arrive at

$$\mathcal{R}_f/\mathcal{L} = \Omega \mathcal{J}^{-1/5}, \tag{3.3}$$

where Ω is a prefactor. Equation (3.3) reveals a relatively weak power-law relationship between the normalized half-width of the filament and the plastocapillary number; as the

plastic effects become larger, the filament spreads less. Generally, the values of prefactor Ω can be a function of gravity, pre-wetted film thickness, elasticity, etc. However, for the range of experimental parameters presented here, Ω can be estimated as a constant, representing the limit of pure plastocapillarity. In the following, we present a thin-film approximation of the present problem, in which we also aim to find the value of Ω.

3.2. *Thin-film approximation*

We apply a lubrication theory for a shallow and inertialess flow of Bingham viscoplastic fluids (shear index $n = 1$) without gravity effects. Following the previous analyses of viscoplastic lubrication theory (Balmforth 2019), and after scaling the length by $\mathcal{L}$, velocity by σ/μ, and time by $\mathcal{L}\mu/\sigma$, we arrive at the following dimensionless depth-integrated evolution equation:

$$h_t = \frac{1}{6}\left[-h_{xxx}Y^2\,(3h - Y)\right]_x, \quad \text{with } Y = \max\left(0,\, h - \mathcal{J}/|h_{xxx}|\right), \tag{3.4}$$

where $h(x, t)$ is the height of the filament, and subscripts denote partial derivatives. In (3.4), $Y(x, t)$ is the yield surface, corresponding to the position in which the stress is equal to the yield stress. When $\mathcal{J} = 0$, we have $Y = h$ and hence (3.4) reduces to the well-known thin-film equation for Newtonian fluids (Oron *et al.* 1997; Craster & Matar 2009). Equation (3.4) represents the planar (two-dimensional) version of the viscoplastic lubrication theory for droplet spreading (Jalaal *et al.* 2021). Note that the dynamics of the thin film spreading likely differs for Herschel–Bulkley fluids where $n \neq 1$; however, the final shape should still be well approximated in the limit studied here.

To explore the dynamics of filament spreading, we solve (3.4) using a finite difference method. In our solution, the length of the domain is large enough such that the filament never arrives at the boundaries. The initial shape of the filament was $h(x, t = 0) = \max(0, 1 - x^2)^3 + h_\infty$ (Jalaal *et al.* 2021). The first and second derivatives of the initial condition are zero at $x = 1$ where it connects the interface of the filament to a pre-wetted film of thickness h_∞ and has a height of almost unity at the centre with zero derivatives. Note that the pre-wetted film removes a genuine triple contact line and the complexities due to stress singularity (Bonn *et al.* 2009; Snoeijer & Andreotti 2013). Figure 4(*a*) shows the numerical solutions of the thin-film equation for $\mathcal{J} = 0.02$. The filament yields fully under surface tension forces at $t = 0$, and spreads on the surface. Later in the process, the influence of yield stress becomes more evident as the surface tension forces decrease. The filament eventually stops deforming when stress inside the filament falls below the yield stress ($Y \to 0$). The variations of half-width $\mathcal{R}(t)$ and maximum height $\mathcal{H}(t)$ of spreading filaments for different plastocapillary numbers are shown in figure 4(*d*,*e*), respectively. In the beginning of the spreading, the dynamics follows the Newtonian spreading (Tanner 1979), for which $\mathcal{R}(t) \sim t^{1/7}$ and $\mathcal{H}(t) \sim t^{-1/7}$, but eventually the curves deviate from the Newtonian limit and approach a constant value that corresponds to the final half-width and height of the filaments. The larger the value of the plastocapillary number, the sooner the filaments approach a final shape. Also, similar to what has been presented in the experiments, the filaments spread less as the value of the plastocapillary number increases.

To compare the theoretical results of the final shapes with the experiments, we use the asymptotic limit of (3.4) for $Y \to 0$, at which the flow is ceased. Hence in dimensional form, we have $\sigma h\, h_{xxx} = \tau_0$. It is more convenient to re-scale the equation at this limit

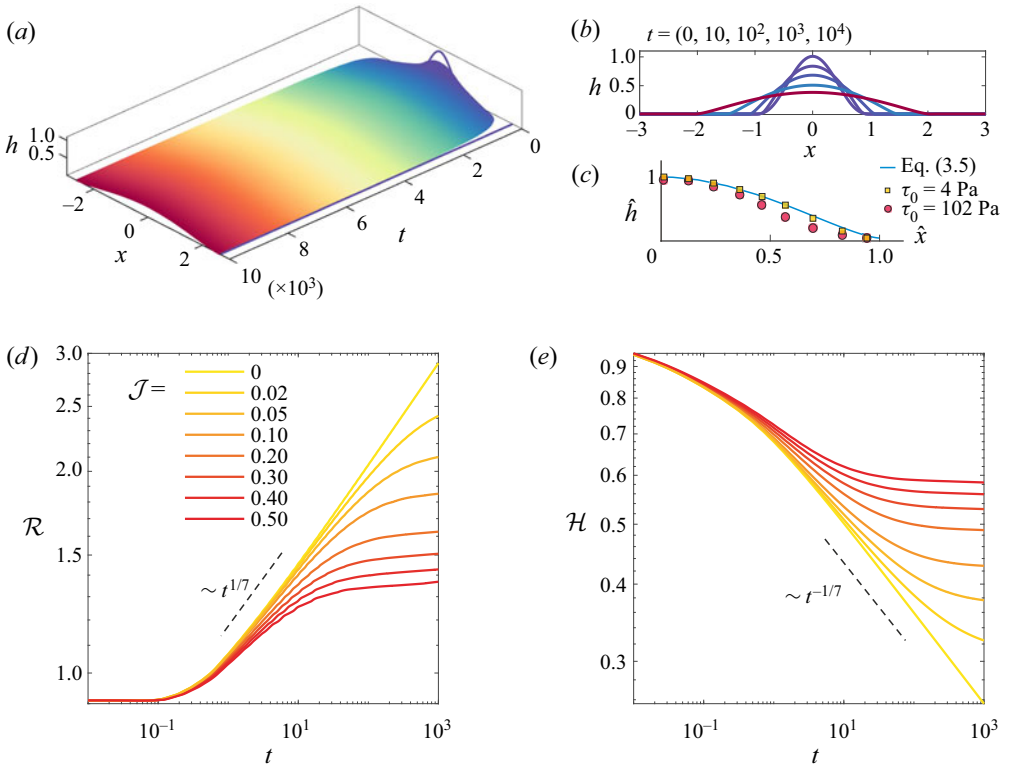

Figure 4. (*a*) Finite difference solution of (3.4). The 3-D dimensional plot is a quasi-representation of a line printing with $\mathcal{J} = 0.02$ at $t = 10^4$. The solid black line notes the final half-width. (*b*) The cross-section of the line at five different times. (*c*) Comparison of the theoretical final shape (where $\hat{h} = h/\mathcal{H}_f$ and $\hat{x} = x/\mathcal{R}_f$) with two experimental examples of samples 1 and 6 at $Q = 10$ ml h^{-1}, where the width and height are normalized with the theoretical prediction. The variations of (*d*) half-width ($\mathcal{R}$) and (*e*) maximum height ($\mathcal{H}$) of the filament are shown as functions of time for different values of $\mathcal{J}$. The dashed black lines show the scaling laws for Newtonian ($\mathcal{J} = 0$) limits.

with final height and half-width, i.e. $\hat{h} = h/\mathcal{H}_f$ and $\hat{x} = x/\mathcal{R}_f$. Hence

$$\hat{h}\,\hat{h}_{\hat{x}\hat{x}\hat{x}} = \Lambda, \quad \text{where } \Lambda = \tau_0 \mathcal{R}_f^3/\sigma \mathcal{H}_f^2. \tag{3.5}$$

The equation above governs the final shape of the filament with constant cross-sectional area $A = 2\mathcal{H}_f \mathcal{R}_f \mathcal{I}$, where $\mathcal{I} = \int_0^1 \hat{h}\,\mathrm{d}\hat{x}$ is *a priori* unknown. From the definitions of Λ and A, we find the same relationship as in (3.3), with $\Omega = (\Lambda/\mathcal{I}^2)^{1/5}$. We solve (3.5) as a boundary value problem (cf. the recent work on droplet spreading for the details of numerical method and boundary conditions, Jalaal *et al.* 2021) to find the final shape of the filament and $\Lambda \approx 3.53$ and $\mathcal{I} \approx 0.58$, and therefore $\Omega \approx 1.59$. Figure 4(*c*) compares the obtained theoretical shape with two examples of experimental data with smallest and largest yield stress. While theory predicts the shape of the fluid with small yield stresses very well (red line versus the OCT image), such agreement is less pronounced for the fluid with a higher yield stress. A comparison of (3.3) with the obtained Ω from the asymptotic analysis above is shown in figure 3(*b*). While the theoretical prediction works fine for small values of $\mathcal{J}$, the comparison suffers from discrepancies at higher values. Fitting the data with a power-law function results in $\mathcal{R}_f/\mathcal{L} = 1.859\mathcal{J}^{-0.156}$, showing the theory

underpredict the prefactor and overpredict the magnitude of the power law by about 15 % and 28 %, respectively. The difference between theory and experiments could be due to both theoretical and experimental limitations. We will discuss these limitations in the next section and provide suggestions for future work.

4. Conclusion and discussion

We have studied experimentally and theoretically the printing mechanism of a single filament of a complex fluid with viscoplastic rheology. The study was focused on the plastocapillarity regime, where surface tension is the driving mechanism and yield stress is the resisting one. The experimental set-up offers a simple configuration to study several fundamental aspects of 3-D printing of complex fluids. Additionally, optical coherence tomography (OCT) provides the opportunity to measure easily and accurately the geometrical features of the filaments, and potentially gives insight into the flow inside the filament. Our primary interest was the final width of the filaments. Theoretically, we solved the viscoplastic lubrication equations governing the cross-sectional spreading of the filaments. We also found a simple scaling law for the final half-width of the filament, $\mathcal{R}_f/\mathcal{L} = 1.59\mathcal{J}^{-1/5}$, where the prefactor was obtained via an asymptotic analysis. Given the complexity of the problem, and the limitations of the model, the comparison between the experimental and theoretical results shows some discrepancy (see figure 3). In experiments, the explicit effects of the pre-wetted film are not yet fully clear. It is expected that a finite thickness of the film affects the spreading (Blackwell *et al.* 2015; Sen, Morales & Ewoldt 2020) and possibly slightly increases the final width of the filament (Jalaal *et al.* 2021). For the present study, we fixed the values of the pre-wetted film at the thinnest thickness available for our experimental conditions. This allowed us to focus on our main goal, finding the final width of the filament in a capillary-driven regime. One extension of the present work could be a systematic study on the effect of the pre-wetted film thickness on the spreading and final shape of the filament. The experiments were also performed on normal glass surfaces. For droplet spreading on solid surfaces, it has been shown that 'apparent slip' could change the dynamics and equilibrium shape of droplets (Jalaal *et al.* 2015; Martouzet *et al.* 2021). Like the pre-wetted film, the 'slippery' condition of the substrate could result in a larger final width. Hence these might explain the underprediction of the theory in figure 3(*b*). Therefore, another extension of the work could then be to study systematically the spreading of filaments on rough or chemically treated surfaces to investigate the effect of 'slip'. The theory presented here ignores the elastic effects. In practice, however, materials feature viscoelastic properties below and above the yield stress. Given that viscoelastic properties can influence the spreading and the final shape of the filament, further investigation is required. A possible extension of our work includes mathematical models with elasto-viscoplastic (EVP) characteristics (Saramito 2007; de Souza Mendes 2011; Dimitriou & McKinley 2014; Saramito & Wachs 2017). Such models could potentially be implemented in thin-film limit or numerical simulations that solve for two phases with moving boundaries (Izbassarov & Tammisola 2020; Sanjay, Lohse & Jalaal 2021). Using EVP models, one should be able to study explicitly different elastic effects. Also note that the presented theory assumes that the cross-sections of the filaments have a large aspect ratio (they are shallow). While this is valid for most of the experimental parameters, for the largest yield stress, this aspect ratio is around 6. The theory could be improved in non-asymptotic fashion, by retaining the full surface curvature or using numerical simulations to go beyond the lubrication limit.

Our work has direct applications in the coating and 3-D printing industries, where spreading and printing filaments of viscoplastic fluids play a key role. However, by studying a single filament of soft yield stress materials, we have not addressed a number of relevant questions in the broad context of 3-D printing. Further extensions of the present study include the spreading and welding (coalescence) of multiple filaments next to each other (Colanges *et al.*, personal communication 2023; Kern, Sæter & Carlson 2022) or on top of each other. Additionally, the regime of very large plastocapillary numbers still requires more investigation, where the deformations due to surface tension are much smaller and localized. Such investigations are required to fully address the printability of ink in relationship to rheology and fluid mechanics of 3-D printing. Moreover, a more systematic study of the flow of viscoplastic fluids near the nozzle, its effects on the filament shapes, printing on dry surfaces when contact angle dynamics plays an important role, and printing more complicated line geometries like corners (Friedrich & Begley 2020) are still required. Finally, the present study focuses mostly on the final state of the filaments. More systematic experimental and theoretical studies on the spreading of filaments with complex rheology are yet to be done to reveal the dynamics of spreading. This is of great importance when the material itself features rheological properties such as shear-thinning, elasticity, aging and thixotropy (Chen *et al.* 2018; Corker *et al.* 2019; Sen *et al.* 2021, 2020), factors that were not studied in the present work.

The OCT easily furnishes cross-sectional images of the filament at small scales and the points it merges to the pre-wetted film. Further improvement of the system can result in simultaneous measurement of the dynamics of the spreading, rheological features of the fluid, and the flow field inside the filaments (Manukyan *et al.* 2013; Trantum *et al.* 2014; Edwards *et al.* 2018; Jalaal *et al.* 2018).

Acknowledgements. We are grateful to N.J. Balmforth for helping with the viscoplastic lubrication theory. We would like to thank N. Schramma, U. Sen, C. Seyfert, V. Sanjay and D. Giesen for useful discussions.

Declaration of interests. The authors report no conflict of interest.

Author ORCIDs.
Maziyar Jalaal https://orcid.org/0000-0002-5654-8505.

References

Ancey, C. 2007 Plasticity and geophysical flows: a review. *J. Non-Newtonian Fluid Mech.* **142** (1–3), 4–35.

Backholm, M., Benzaquen, M., Salez, T., Raphaël, E. & Dalnoki-Veress, K. 2014 Capillary levelling of a cylindrical hole in a viscous film. *Soft Matt.* **10** (15), 2550–2558.

Balmforth, N.J. 2019 Viscoplastic asymptotics and other analytical methods. In *Lectures on Visco-Plastic Fluid Mechanics* (ed. G. Ovarlez & S. Hormozi), pp. 41–82. Springer.

Balmforth, N.J., Frigaard, I.A. & Ovarlez, G. 2014 Yielding to stress: recent developments in viscoplastic fluid mechanics. *Annu. Rev. Fluid Mech.* **46**, 121–146.

Barnes, H.A. 1999 The yield stress – a review or '$\pi\alpha\nu\tau\alpha\ \rho\varepsilon\iota$' – everything flows? *J. Non-Newtonian Fluid Mech.* **81** (1–2), 133–178.

Bergemann, N., Juel, A. & Heil, M. 2018 Viscous drops on a layer of the same fluid: from sinking, wedging and spreading to their long-time evolution. *J. Fluid Mech.* **843**, 1–28.

Bird, R.B., Armstrong, R.C. & Hassager, O. 1987 *Dynamics of Polymeric Liquids. Vol. 1: Fluid Mechanics*. Wiley.

Blackwell, B.C., Deetjen, M.E., Gaudio, J.E. & Ewoldt, R.H. 2015 Sticking and splashing in yield-stress fluid drop impacts on coated surfaces. *Phys. Fluids* **27** (4), 043101.

Bonn, D., Denn, M.M., Berthier, L., Divoux, T. & Manneville, S. 2017 Yield stress materials in soft condensed matter. *Rev. Mod. Phys.* **89** (3), 035005.

Bonn, D., Eggers, J., Indekeu, J., Meunier, J. & Rolley, E. 2009 Wetting and spreading. *Rev. Mod. Phys.* **81** (2), 739–805.

BRUTIN, D., ZHU, Z., RAHLI, O., XIE, J., LIU, Q. & TADRIST, L. 2009 Sessile drop in microgravity: creation, contact angle and interface. *Microgravity Sci. Technol.* **21** (1), 67–76.

BUSWELL, R.A., DE SILVA, W.R.L., JONES, S.Z. & DIRRENBERGER, J. 2018 3D printing using concrete extrusion: a roadmap for research. *Cement Concrete Res.* **112**, 37–49.

CHEN, Y., WANG, Y., YANG, Q., LIAO, Y., ZHU, B., ZHAO, G., SHEN, R., LU, X. & QU, S. 2018 A novel thixotropic magnesium phosphate-based bioink with excellent printability for application in 3D printing. *J. Mater. Chem.* B **6** (27), 4502–4513.

CORKER, A., NG, H.C.-H., POOLE, R.J. & GARCÍA-TUÑÓN, E. 2019 3D printing with 2D colloids: designing rheology protocols to predict 'printability' of soft-materials. *Soft Matt.* **15** (6), 1444–1456.

COUSSOT, P. 2014 Yield stress fluid flows: a review of experimental data. *J. Non-Newtonian Fluid Mech.* **211**, 31–49.

CRASTER, R.V. & MATAR, O.K. 2009 Dynamics and stability of thin liquid films. *Rev. Mod. Phys.* **81** (3), 1131.

DANESHI, M., POURZAHEDI, A., MARTINEZ, D.M. & GRECOV, D. 2019 Characterising wall-slip behaviour of Carbopol gels in a fully-developed Poiseuille flow. *J. Non-Newtonian Fluid Mech.* **269**, 65–72.

DERBY, B. 2010 Inkjet printing of functional and structural materials: fluid property requirements, feature stability, and resolution. *Annu. Rev. Mater. Res.* **40**, 395–414.

DIANA, A., CASTILLO, M., BRUTIN, D. & STEINBERG, T. 2012 Sessile drop wettability in normal and reduced gravity. *Microgravity Sci. Technol.* **24** (3), 195–202.

DIMITRIOU, C.J. & MCKINLEY, G.H. 2014 A comprehensive constitutive law for waxy crude oil: a thixotropic yield stress fluid. *Soft Matt.* **10** (35), 6619–6644.

DINKGREVE, M., PAREDES, J., DENN, M.M. & BONN, D. 2016 On different ways of measuring 'the' yield stress. *J. Non-Newtonian Fluid Mech.* **238**, 233–241.

DONLEY, G.J., SINGH, P.K., SHETTY, A. & ROGERS, S.A. 2020 Elucidating the G'' overshoot in soft materials with a yield transition via a time-resolved experimental strain decomposition. *Proc. Natl Acad. Sci. USA* **117** (36), 21945–21952.

DUBASH, N., BALMFORTH, N.J., SLIM, A.C. & COCHARD, S. 2009 What is the final shape of a viscoplastic slump? *J. Non-Newtonian Fluid Mech.* **158** (1–3), 91–100.

D'ANGELO, O., KUTHE, F., VAN NIEUWLAND, K., EDERVEEN JANSSEN, C., VOIGTMANN, T. & JALAAL, M. 2022 Spreading of droplets under various gravitational accelerations. *Rev. Sci. Instrum.* **93** (11), 115103.

EDWARDS, A.M.J., ATKINSON, P.S., CHEUNG, C.S., LIANG, H., FAIRHURST, D.J. & OUALI, F.F. 2018 Density-driven flows in evaporating binary liquid droplets. *Phys. Rev. Lett.* **121** (18), 184501.

EOM, Y., KIM, F., YANG, S.E., SON, J.S. & CHAE, H.G. 2019 Rheological design of 3D printable all-inorganic inks using BiSbTe-based thermoelectric materials. *J. Rheol.* **63** (2), 291–304.

EWOLDT, R.H. & SAENGOW, C. 2021 Designing complex fluids. *Annu. Rev. Fluid Mech.* **54**, 413–441.

FAES, M., VALKENAERS, H., VOGELER, F., VLEUGELS, J. & FERRARIS, E. 2015 Extrusion-based 3D printing of ceramic components. *Proc. CIRP* **28**, 76–81.

FERCHER, A.F., DREXLER, W., HITZENBERGER, C.K. & LASSER, T. 2003 Optical coherence tomography – principles and applications. *Rep. Prog. Phys.* **66** (2), 239.

FLATT, R.J., LAROSA, D. & ROUSSEL, N. 2006 Linking yield stress measurements: spread test versus viskomat. *Cement Concrete Res.* **36** (1), 99–109.

FRIEDRICH, L. & BEGLEY, M. 2020 Corner accuracy in direct ink writing with support material. *Bioprinting* **19**, e00086.

GARG, A., BERGEMANN, N., SMITH, B., HEIL, M. & JUEL, A. 2021 Fluidisation of yield stress fluids under vibration. *J. Non-Newtonian Fluid Mech.* **294**, 104595.

GERMAN, G. & BERTOLA, V. 2010 The spreading behaviour of capillary driven yield-stress drops. *Colloids Surf. (*A*)* **366** (1–3), 18–26.

GNANASEKARAN, K., HEIJMANS, T., VAN BENNEKOM, S., WOLDHUIS, H., WIJNIA, S., DE WITH, G. & FRIEDRICH, H. 2017 3D printing of CNT- and graphene-based conductive polymer nanocomposites by fused deposition modeling. *Appl. Mater. Today* **9**, 21–28.

GOSSELIN, C., DUBALLET, R., ROUX, P., GAUDILLIÈRE, N., DIRRENBERGER, J. & MOREL, P. 2016 Large-scale 3D printing of ultra-high performance concrete – a new processing route for architects and builders. *Mater. Des.* **100**, 102–109.

IZBASSAROV, D. & TAMMISOLA, O. 2020 Dynamics of an elastoviscoplastic droplet in a Newtonian medium under shear flow. *Phys. Rev. Fluids* **5** (11), 113301.

JALAAL, M., BALMFORTH, N.J. & STOEBER, B. 2015 Slip of spreading viscoplastic droplets. *Langmuir* **31** (44), 12071–12075.

JALAAL, M., KEMPER, D. & LOHSE, D. 2019*a* Viscoplastic water entry. *J. Fluid Mech.* **864**, 596–613.

JALAAL, M., SCHAARSBERG, M.K., VISSER, C.-W. & LOHSE, D. 2019*b* Laser-induced forward transfer of viscoplastic fluids. *J. Fluid Mech.* **880**, 497–513.

JALAAL, M., SEYFERT, C. & SNOEIJER, J.H. 2019*c* Capillary ripples in thin viscous films. *J. Fluid Mech.* **880**, 430–440.

JALAAL, M., SEYFERT, C., STOEBER, B. & BALMFORTH, N.J. 2018 Gel-controlled droplet spreading. *J. Fluid Mech.* **837**, 115–128.

JALAAL, M., STOEBER, B. & BALMFORTH, N.J. 2021 Spreading of viscoplastic droplets. *J. Fluid Mech.* **914**, A21.

JIANG, Y., JOSHUA, A., DING, L., WANG, B., FENG, X., MAO, Z., XU, H. & SUI, X. 2020 Rheology of regenerated cellulose suspension and influence of sodium alginate. *Intl J. Biol. Macromol.* **148**, 811–816.

JØRGENSEN, L., LE MERRER, M., DELANOË-AYARI, H. & BARENTIN, C. 2015 Yield stress and elasticity influence on surface tension measurements. *Soft Matt.* **11** (25), 5111–5121.

KERN, V.R., SÆTER, T. & CARLSON, A. 2022 Viscoplastic sessile drop coalescence. *Phys. Rev. Fluids* **7** (8), L081601.

KIM, J.-Y., SONG, J.-Y., LEE, E.-J. & PARK, S.-K. 2003 Rheological properties and microstructures of Carbopol gel network system. *Colloid Polym. Sci.* **281** (7), 614–623.

KIYOTAKE, E.A., DOUGLAS, A.W., THOMAS, E.E., NIMMO, S.L. & DETAMORE, M.S. 2019 Development and quantitative characterization of the precursor rheology of hyaluronic acid hydrogels for bioprinting. *Acta Biomater.* **95**, 176–187.

KOLDEWEIJ, R.B.J., KANT, P., HARTH, K., DE RUITER, R., GELDERBLOM, H., SNOEIJER, J.H., LOHSE, D. & VAN LIMBEEK, M.A.J. 2021 Initial solidification dynamics of spreading droplets. *Phys. Rev. Fluids* **6** (12), L121601.

LEWIS, J.A. 2006 Direct ink writing of 3D functional materials. *Adv. Funct. Mater.* **16** (17), 2193–2204.

LIU, Y., BALMFORTH, N.J., HORMOZI, S. & HEWITT, D.R. 2016 Two-dimensional viscoplastic dambreaks. *J. Non-Newtonian Fluid Mech.* **238**, 65–79.

LOHSE, D. 2022 Fundamental fluid dynamics challenges in inkjet printing. *Annu. Rev. Fluid Mech.* **54**, 349–382.

LUU, L.-H. & FORTERRE, Y. 2009 Drop impact of yield-stress fluids. *J. Fluid Mech.* **632**, 301–327.

MACKAY, M.E. 2018 The importance of rheological behavior in the additive manufacturing technique material extrusion. *J. Rheol.* **62** (6), 1549–1561.

MANUKYAN, S., SAUER, H.M., ROISMAN, I.V., BALDWIN, K.A., FAIRHURST, D.J., LIANG, H., VENZMER, J. & TROPEA, C. 2013 Imaging internal flows in a drying sessile polymer dispersion drop using spectral radar optical coherence tomography (SR-OCT). *J. Colloid Interface Sci.* **395**, 287–293.

MARTOUZET, G., JØRGENSEN, L., PELET, Y., BIANCE, A.-L. & BARENTIN, C. 2021 Dynamic arrest during the spreading of a yield stress fluid drop. *Phys. Rev. Fluids* **6** (4), 044006.

DEL MAZO-BARBARA, L. & GINEBRA, M.-P. 2021 Rheological characterisation of ceramic inks for 3D direct ink writing: a review. *J. Eur. Ceram. Soc.* **41** (16), 18–33.

M'BARKI, A., BOCQUET, L. & STEVENSON, A. 2017 Linking rheology and printability for dense and strong ceramics by direct ink writing. *Sci. Rep.* **7** (1), 1–10.

MOUSER, V.H.M., MELCHELS, F.P.W., VISSER, J., DHERT, W.J.A., GAWLITTA, D. & MALDA, J. 2016 Yield stress determines bioprintability of hydrogels based on gelatin-methacryloyl and gellan gum for cartilage bioprinting. *Biofabrication* **8** (3), 035003.

NGO, T.D., KASHANI, A., IMBALZANO, G., NGUYEN, K.T.Q. & HUI, D. 2018 Additive manufacturing (3D printing): a review of materials, methods, applications and challenges. *Compos. Part* B*: Engng* **143**, 172–196.

O'BRYAN, C.S., BHATTACHARJEE, T., NIEMI, S.R., BALACHANDAR, S., BALDWIN, N., ELLISON, S.T., TAYLOR, C.R., SAWYER, W.G. & ANGELINI, T.E. 2017 Three-dimensional printing with sacrificial materials for soft matter manufacturing. *MRS Bull.* **42** (8), 571–577.

OISHI, C.M., THOMPSON, R.L. & MARTINS, F.P. 2019*a* Impact of capillary drops of complex fluids on a solid surface. *Phys. Fluids* **31** (12), 123109.

OISHI, C.M., THOMPSON, R.L. & MARTINS, F.P. 2019*b* Normal and oblique drop impact of yield stress fluids with thixotropic effects. *J. Fluid Mech.* **876**, 642–679.

ORON, A., DAVIS, S.H. & BANKOFF, S.G. 1997 Long-scale evolution of thin liquid films. *Rev. Mod. Phys.* **69** (3), 931.

PAXTON, N., SMOLAN, W., BÖCK, T., MELCHELS, F., GROLL, J. & JUNGST, T. 2017 Proposal to assess printability of bioinks for extrusion-based bioprinting and evaluation of rheological properties governing bioprintability. *Biofabrication* **9** (4), 044107.

PLACONE, J.K. & ENGLER, A.J. 2018 Recent advances in extrusion-based 3D printing for biomedical applications. *Adv. Healthc. Mater.* **7** (8), 1701161.

POSTIGLIONE, G., NATALE, G., GRIFFINI, G., LEVI, M. & TURRI, S. 2015 Conductive 3D microstructures by direct 3D printing of polymer/carbon nanotube nanocomposites via liquid deposition modeling. *Compos. Part* A*: Appl. Sci. Manuf.* **76**, 110–114.

RODELL, C.B., KAMINSKI, A.L. & BURDICK, J.A. 2013 Rational design of network properties in guest–host assembled and shear-thinning hyaluronic acid hydrogels. *Biomacromolecules* **14** (11), 4125–4134.

ROUSSEL, N. & COUSSOT, P. 2005 'Fifty-cent rheometer' for yield stress measurements: from slump to spreading flow. *J. Rheol.* **49** (3), 705–718.

SAÏDI, A., MARTIN, C. & MAGNIN, A. 2010 Influence of yield stress on the fluid droplet impact control. *J. Non-Newtonian Fluid Mech.* **165** (11–12), 596–606.

SANJAY, V., LOHSE, D. & JALAAL, M. 2021 Bubble bursting in viscoplastic medium. *J. Fluid Mech.* **922**, A2.

SARAMITO, P. 2007 A new constitutive equation for elastoviscoplastic fluid flows. *J. Non-Newtonian Fluid Mech.* **145** (1), 1–14.

SARAMITO, P. & WACHS, A. 2017 Progress in numerical simulation of yield stress fluid flows. *Rheol. Acta* **56** (3), 211–230.

SEN, S., MORALES, A.G. & EWOLDT, R.H. 2020 Viscoplastic drop impact on thin films. *J. Fluid Mech.* **891**.

SEN, S., MORALES, A.G. & EWOLDT, R.H. 2021 Thixotropy in viscoplastic drop impact on thin films. *Phys. Rev. Fluids* **6** (4), 043301.

SIACOR, F.D.C., CHEN, Q., ZHAO, J.Y., HAN, L., VALINO, A.D., TABOADA, E.B., CALDONA, E.B. & ADVINCULA, R.C. 2021 On the additive manufacturing (3D printing) of viscoelastic materials and flow behavior: from composites to food manufacturing. *Addit. Manuf.* **45**, 102043.

SIQUEIRA, G., KOKKINIS, D., LIBANORI, R., HAUSMANN, M.K., GLADMAN, A.S., NEELS, A., TINGAUT, P., ZIMMERMANN, T., LEWIS, J.A. & STUDART, A.R. 2017 Cellulose nanocrystal inks for 3D printing of textured cellular architectures. *Adv. Funct. Mater.* **27** (12), 1604619.

SNOEIJER, J.H. & ANDREOTTI, B. 2013 Moving contact lines: scales, regimes, and dynamical transitions. *Annu. Rev. Fluid Mech.* **45**, 269–292.

DE SOUZA MENDES, P.R. 2011 Thixotropic elasto-viscoplastic model for structured fluids. *Soft Matt.* **7** (6), 2471–2483.

SUN, Q., YANG, Z., CHENG, H., PENG, Y., HUANG, Y. & CHEN, M. 2018 Creation of three-dimensional structures by direct ink writing with kaolin suspensions. *J. Mater. Chem.* C **6** (42), 11392–11400.

TAGLIAFERRI, S., PANAGIOTOPOULOS, A. & MATTEVI, C. 2021 Direct ink writing of energy materials. *Mater. Adv.* **2** (2), 540–563.

TANNER, L.H. 1979 The spreading of silicone oil drops on horizontal surfaces. *J. Phys.* D*: Appl. Phys.* **12** (9), 1473.

TAVAKOLI, F., DAVIS, S.H. & KAVEHPOUR, H.P. 2014 Spreading and arrest of a molten liquid on cold substrates. *Langmuir* **30** (34), 10151–10155.

TRANTUM, J.R., BAGLIA, M.L., EAGLETON, Z.E., MERNAUGH, R.L. & HASELTON, F.R. 2014 Biosensor design based on Marangoni flow in an evaporating drop. *Lab on a Chip* **14** (2), 315–324.

TUCK, E.O. & SCHWARTZ, L.W. 1990 A numerical and asymptotic study of some third-order ordinary differential equations relevant to draining and coating flows. *SIAM Rev.* **32** (3), 453–469.

UPPAL, A.S., CRASTER, R.V. & MATAR, O.K. 2017 Dynamics of spreading thixotropic droplets. *J. Non-Newtonian Fluid Mech.* **240**, 1–14.

VALETTE, R., PEREIRA, A., RIBER, S., SARDO, L., LARCHER, A. & HACHEM, E. 2021 Viscoplastic dam-breaks. *J. Non-Newtonian Fluid Mech.* **287**, 104447.

VALINO, A.D., DIZON, J.R.C., ESPERA, A.H. JR., CHEN, Q., MESSMAN, J. & ADVINCULA, R.C. 2019 Advances in 3D printing of thermoplastic polymer composites and nanocomposites. *Prog. Polym. Sci.* **98**, 101162.

WILSON, S.A., CROSS, L.M., PEAK, C.W. & GAHARWAR, A.K. 2017 Shear-thinning and thermo-reversible nanoengineered inks for 3D bioprinting. *ACS Appl. Mater. Interfaces* **9** (50), 43449–43458.

ZHANG, D., CHI, B., LI, B., GAO, Z., DU, Y., GUO, J. & WEI, J. 2016 Fabrication of highly conductive graphene flexible circuits by 3D printing. *Synth. Met.* **217**, 79–86.

ZHU, S., STIEGER, M.A., VAN DER GOOT, A.J. & SCHUTYSER, M.A.I. 2019 Extrusion-based 3D printing of food pastes: correlating rheological properties with printing behaviour. *Innov. Food Sci. Emerg.* **58**, 102214.